Inorg. Chem. **2007**, *46*, 874–883

Diverse Polyanions Based on $MnBi_4$ and $MnSb_4$ Tetrahedra: Polymorphism, Structure, and Bonding in $Ca_{21}Mn_4Bi_{18}$ and $Ca_{21}Mn_4Sb_{18}$

Sheng-qing Xia and Svilen Bobev*

Department of Chemistry and Biochemistry, University of Delaware, Newark, Delaware 19716

Received October 12, 2006

New transition-metal-containing Zintl phases, $Ca_{21}Mn_4Bi_{18}$ and $Ca_{21}Mn_4Sb_{18}$, have been synthesized by high-temperature reactions, and their structures have been determined by single-crystal X-ray diffraction. $Ca_{21}Mn_4Bi_{18}$ crystallizes in the monoclinic space group *C*2/*c* (No. 15, $Z = 4$) with $a = 17.470(2)$ Å, $b = 17.392(2)$ Å, $c = 17.208(2)$ Å, $\beta = 93.253(2)°$ (R1 = 0.0405, wR2 = 0.0840) and is isostructural with the recently reported $Ca_{21}Mn_4Sb_{18}$. The compound with the same formula, which is also reported herein, is in turn a new polymorph of $Ca_{21}Mn_4Sb_{18}$ and crystallizes in the monoclinic space group *C*2/*m* (No. 12, $Z = 4$) with $a = 17.415(6)$ Å, $b = 16.567(6)$ Å, $c = 17.047(6)$ Å, $\beta = 92.068(4)°$ (R1 = 0.0432, wR2 = 0.0788). This new polymorph of $Ca_{21}Mn_4Sb_{18}$ is isostructural with another related compound, $Sr_{21}Mn_4Sb_{18}$. Despite the similarity in their chemical formulas, the structures of $Ca_{21}Mn_4Bi_{18}$ and $Ca_{21}Mn_4Sb_{18}$ are very different: $Ca_{21}Mn_4Bi_{18}$ contains unique $[Mn_4Bi_{10}]$ cluster anions made up of four $MnBi_4$ tetrahedra connected through edge-sharing. The structure of $Ca_{21}Mn_4Sb_{18}$ features edge- and corner-shared $MnSb_4$ tetrahedra, which make $[Mn_4Sb_{11}]$ tetramers. The latter are linked to each other through external Sb–Sb bonds to form larger isolated $[Mn_8Sb_{22}]$ polyanions. Electronic band structure calculations performed using the TB-LMTO-ASA method show a small band gap at the Fermi level, suggesting narrow-gap semiconducting behavior for both compounds.

Introduction

Various manganese-based inorganic materials exhibit a wealth of interesting chemical and physical properties and have recently become the subject of much attention by scientists from different disciplines. Several specific examples, which are important not only from a purely scientific point of view but also have great technological significance include (1) the oxides $La_{1-x}Ca_xMnO_3$ and $Tl_2Mn_2O_7$, which have been reported as illustrious examples of "giant" or "colossal" magnetoresistive (GMR or CMR) materials;[1,2] (2) some half-Heusler TMnSb phases (T = transition metal), which are frequently associated with the half-metallic ferromagnets[3] and exhibit very high Curie temperatures; (3) Mn-doped semiconductors of the III−V type, such as $Ga_{1-x}Mn_xPn$, (Pn = pnicogen),[4] often referred to as dilute magnetic semiconductors, which are promising candidates for applications in magnetic sensors and magneto-electronic (spintronic) devices;[5] and (4) the itinerant ferromagnet MnSi, which shows signs of well-defined anomalies near the quantum critical point,[6] etc.

In addition to these, there are also several other types of manganese-containing intermetallics, such as $Ca_{14}MnBi_{11}$,[7] $Ca_9Mn_4Bi_9$,[8] $Sr_{21}Mn_4Sb_{18}$,[9] $Ca_{21}Mn_4Sb_{18}$,[10] $Eu_{10}Mn_6Sb_{13}$,[11] $CaMn_2Sb_2$,[12] Sr_2MnSb_2,[13] etc., whose structures are based

* To whom correspondence should be addressed. E-mail: sbobev@chem.udel.edu. Phone: (302) 831-8720. Fax: (302) 831-6335.

(1) Zhao, G. M.; Conder, K.; Keller, H.; Muller, K. A. *Nature* **1996**, *381*, 676−678.
(2) Ramirez, A. P.; Subramanian, M. A. *Science* **1997**, *277*, 546−549.
(3) (a) de Groot, R. A.; Mueller, F. M.; Vanengen, P. G.; Buschow, K. H. J. *Phys. Rev. Lett.* **1983**, *50*, 2024−2027. (b) Orgassa, D.; Fujiwara, H.; Schulthess, T. C.; Butler, W. H. *Phys. Rev. B: Condens. Matter* **1999**, *60*, 13237−13240.
(4) (a) Edmonds, K. W; Campion, R. P.; Wang, K. Y.; Neumann, A. C.; Gallagher, B. L.; Foxon, C. T.; Main, P. C. *J. Appl. Phys.* **2003**, *93*, 6787−6789. (b) Burch, K. S; Shrekenhamer, D. B.; Singley, E. J.; Stephens, J.; Sheu, B. L.; Kawakami, R. K.; Schiffer, P.; Samarth, N.; Awschalom, D. D.; Basov, D. N. *Phys. Rev. Lett.* **2006**, *97*, 087208.
(5) Prinz, G. A. *Science* **1998**, *282*, 1660−1663.
(6) Doiron-Leyraud, N.; Walker, I. R.; Taillefer, L.; Steiner, M. J.; Julian, S. R.; Lonzarich, G. G. *Nature* **2003**, *425*, 595−599.
(7) Kuromoto, T. Y.; Kauzlarich, S. M.; Webb, D. J. *Chem. Mater.* **1992**, *4*, 435−440.
(8) Brechetel, E.; Cordier, G.; Schäfer, H. Z. *Naturforsch.* **1979**, *34B*, 1229−1233.
(9) Kim, H.; Condron, C. L.; Holm, A. P.; Kauzlarich, S. M. *J. Am. Chem. Soc.* **2000**, *122*, 10720−10721.
(10) Holm, A. P.; Olmstead, M. M.; Kauzlarich, S. M. *Inorg. Chem.* **2003**, *42*, 1973−1981.

10.1021/ic061958j CCC: $37.00
Published on Web 01/05/2007

on isolated or interlinked $MnBi_4$ or $MnSb_4$ tetrahedra with alkaline-earth or rare-earth cations filling the space between them. Notably, these complex structures can simply be rationalized using the Zintl concept,[14] i.e., by assuming a complete valence electron transfer from the electropositive elements to the electronegative ones, whereby each element achieves a closed-shell state conforming to the octet rule. In all of the above-mentioned compounds, the magnetic and the electronic properties are governed by diverse Mn−Mn interactions that are strongly dependent on various structural parameters such as the Mn−Mn distances, the topology of the polyanionic subnetwork, and/or the identity of the cations. For instance, in the $A_{14}MnPn_{11}$ series alone (A = Ca, Sr, Ba, Eu, Yb; Pn = P, As, Sb, Bi),[15] the Mn spins can be either antiferromagnetically or ferromagnetically coupled, whereas the electronic conductivity can vary within several orders of magnitude. Recent work also shows colossal magnetoresistance and high thermoelectric figure of merit for some members of this family.[16]

Intrigued by the rich phenomenology of these structurally related phases, we undertook systematic studies in the Ca−Mn−Bi and Ca−Mn−Sb systems. This work is part of a broader program aimed at better understanding the structural complexity in such compounds and determining how the Mn−Mn interactions at the atomic level influence the macroscopic physical properties. These efforts were focused primarily on the synthesis of new Zintl-like compounds, whose structures are based on Mn-centered Bi_4 or Sb_4 tetrahedra. Up until now, our studies have proven successful,[12] and herein we report a study of the structure and the bonding in two new phases, $Ca_{21}Mn_4Bi_{18}$ and $Ca_{21}Mn_4Sb_{18}$. Despite the identical chemical formulas, both compounds crystallize in two different structure types. $Ca_{21}Mn_4Bi_{18}$ is isostructural with the recently reported $Ca_{21}Mn_4Sb_{18}$ (α-$Ca_{21}Mn_4Sb_{18}$ hereafter),[10] whereas $Ca_{21}Mn_4Sb_{18}$ we report is a new polymorph (β-$Ca_{21}Mn_4Sb_{18}$ hereafter) and it is isostructural with another related compound, $Sr_{21}Mn_4Sb_{18}$.[9] The two structures are based on unique cluster anions made up of $MnBi_4$ or $MnSb_4$ tetrahedra, and the structural relationships between them are discussed. In addition, we also report the temperature and field-dependent dc magnetization and the TB-LMTO-ASA spin-polarized band structure calculations, which provide further insight into the bonding and the properties of these new compounds.

Experimental Section

Synthesis. Handling of all materials was carried out inside an argon-filled glove box or under vacuum. All elements for the syntheses were used as received: Ca (Aldrich, granules, 99.9%), Mn (Alfa, pieces, 99.98%), Bi (Alfa, rod, 99.99%), and Sb (Alfa, shot, 99.99%). Two different synthetic procedures were explored—on-stoichiometry reactions in welded Nb tubes or flux reactions in alumina crucibles. Specific temperature profiles are mentioned below; further details on the techniques and the experimental procedures are given elsewhere.[12]

$Ca_{21}Mn_4Bi_{18}$. Small, air-sensitive crystals of $Ca_{21}Mn_4Bi_{18}$ were identified from a reaction of the elements in a sealed Nb tube. The reaction mixture (with 3-fold excess of Mn to avoid the formation of the binary phase $Ca_{11}Bi_{10}$[17]) was heated to 1100 °C at a rate of 100 °C/h, homogenized at 1100 °C for 24 h, and quickly cooled down to 600 °C over 4 h. Then, it was allowed to dwell at this temperature for a week, followed by a cooling step to room temperature at a rate of 60 °C/h. The reaction yielded dark-to-black crystals with irregular shapes identified by powder and single-crystal diffraction as $Ca_{14}MnBi_{11}$,[7] $Ca_9Mn_4Bi_9$,[8] and $Ca_{21}Mn_4Bi_{18}$, respectively. Subsequently, many attempts to synthesize pure phase $Ca_{21}Mn_4Bi_{18}$ were undertaken but proved unsuccessful—almost exclusively, the products of all these reactions contained considerable amounts of $Ca_{14}MnBi_{11}$. Attempts to grow crystals of $Ca_{21}Mn_4Bi_{18}$ from Sn and Pb fluxes failed as well. The major products of these syntheses were $Ca_{11}Bi_{10}$[17] and again $Ca_{14}MnBi_{11}$.[7]

$Ca_{21}Mn_4Sb_{18}$. Small, irregularly shaped crystals of the new β-$Ca_{21}Mn_4Sb_{18}$ polymorph were serendipitously discovered as a minor product of an analogous reaction between Ca, Mn, and Sb in a welded Nb tube. The temperature profile employed in this synthesis was identical to the one described above for $Ca_{21}Mn_4Bi_{18}$. Numerous tries to synthesize this compound in large yields by varying the nominal composition or changing the reaction temperature failed—the major product of almost all on-stoichiometry reactions was $Ca_{14}MnSb_{11}$.[15a] Flux reactions were also explored but proved unsuccessful. However, it must be noted that the use of molten Sn as a solvent does allow for the effective growth of crystals of α-$Ca_{21}Mn_4Sb_{18}$, and the optimized conditions for this flux synthesis have been described in an earlier publication.[10]

The crystals of both $Ca_{21}Mn_4Bi_{18}$ and β-$Ca_{21}Mn_4Sb_{18}$ are very brittle. Their surfaces tarnish in air, which is a sign of slow decomposition/oxidation.

Powder X-ray Diffraction. X-ray powder diffraction patterns were taken at room temperature on a Rigaku MiniFlex powder diffractometer, enclosed in a glove box and using monochromatized Cu Kα radiation. Data were collected in a $\theta-\theta$ mode ($2\theta_{max}$ = 80°) with a step-size of 0.02° and 10 s/step counting time. Samples were ground and prepared inside the glove box to prevent oxidation. JADE and GSAS software packages were used to analyze the

(11) (a) Holm, A. P.; Park, S.-M.; Condron, C. L.; Kim, H.; Klavins, P.; Grandjean, F.; Hermann, R. P.; Long G. J.; Kanatzidis, M. G.; Kauzlarich, S. M.; Kim, S.-J. *Inorg. Chem.* **2003**, *42*, 4660−4667. (b) Brown, D. E.; Johnson, C. E.; Grandjean, F.; Hermann, R. P.; Kauzlarich, S. M.; Holm, A. P.; Long, G. J. *Inorg. Chem.* **2004**, *43*, 1229−1234.

(12) Bobev, S.; Merz, J.; Lima, A.; Fritsch, V.; Thompson, J. D.; Sarrao, J. L.; Gillessen, M.; Dronskowski, R. *Inorg. Chem.* **2006**, *45*, 4047−4054.

(13) Park, S.-M.; Kim, S.-J.; Kanatzidis, M. G. *Inorg. Chem.* **2005**, *44*, 4979−4982.

(14) (a) Zintl, E. *Angew. Chem.* **1939**, *52*, 1−6. (b) Nesper, R. *Prog. Solid State Chem.* **1990**, *20*, 1−45. (c) Eisenmann, B.; Cordier, G. In *Chemistry, Structure, and Bonding of Zintl Phases and Ions*; Kauzlarich, S. M., Ed.; VCH Publishers: New York, 1996; p 61.

(15) (a) Rehr, A.; Kuromoto, T. Y.; Kauzlarich, S. M.; Delcastillo, J.; Webb, D. J. *Chem. Mater.* **1992**, *4*, 435−440. (b) Rehr, A.; Kuromoto, T. Y.; Kauzlarich, S. M.; Delcastillo, J.; Webb, D. J. *Chem. Mater.* **1994**, *6*, 93−99. (c) Chan, J. Y.; Wang, M. E.; Rehr, A.; Kauzlarich, S. M.; Webb, D. J. *Chem. Mater.* **1997**, *9*, 2131−2138. (d) Chan, J. Y.; Kauzlarich, S. M.; Klavins, P.; Shelton, R. N.; Webb, D. J. *Chem. Mater.* **1997**, *9*, 3132−3135. (e) Chan, J. Y.; Kauzlarich, S. M.; Klavins, P.; Shelton, R. N.; Webb, D. J. *Phys. Rev. B* **1998**, *57*, 8103−8106. (f) Chan, J. Y.; Olmstead, M. M.; Kauzlarich, S. M.; Webb, D. J. *Chem. Mater.* **1998**, *10*, 3583−3588. (g) Ratai, E.; Bruins, P.; Hernandez, C. J.; Kauzlarich, S. M.; Augustine, M. P. *Chem. Mater.* **2002**, *14*, 2467−2475. (h) Kim, H.; Kauzlarich, S. M. *J. Solid-State Chem.* **2005**, *178*, 1935.

(16) Brown, S. R.; Kauzlarich, S. M.; Gascoin, F.; Snyder, G. J. *Chem. Mater.* **2006**, *18*, 1873−1877.

(17) Deller, K.; Eisenmann, B. Z. *Naturforsch. B: Chem. Sci.* **1976**, *31*, 29−34.

Table 1. Selected Crystal Data and Structure Refinement Parameters for $Ca_{21}Mn_4Bi_{18}$ and β-$Ca_{21}Mn_4Sb_{18}$

empirical formula	$Ca_{21}Mn_4Bi_{18}$	$Ca_{21}Mn_4Sb_{18}$
fw	4823.08 g/mol	3252.94 g/mol
data collection temp	−153(2) °C	
Radiation, wavelength	Mo Kα, $\lambda = 0.71073$ Å	
cryst syst	monoclinic	
space group	*C*2/*c* (No. 15)	*C*2/*m* (No. 12)
unit cell dimens	$a = 17.470(2)$ Å	$a = 17.415(6)$ Å
	$b = 17.392(2)$ Å	$b = 16.567(6)$ Å
	$c = 17.208(2)$ Å	$c = 17.047(6)$ Å
	$\beta = 93.253(2)°$	$\beta = 92.068(4)°$
unit cell vol, *Z*	5219.9(11) Å^3, 4	4915(3) Å^3, 4
density (ρ_{calc})	6.137 g/cm^3	4.396 g/cm^3
abs coeff (μ)	63.416 mm^{-1}	12.885 mm^{-1}
final *R* indices[a] [$I > 2\sigma(I)$]	R1 = 0.0405	R1 = 0.0432
	wR2 = 0.0840	wR2 = 0.0788
final *R* indices[a] [all data]	R1 = 0.0556	R1 = 0.0598
	wR2 = 0.0894	wR2 = 0.0853

[a] $R1 = \sum||F_o| - |F_c||/\sum|F_o|$; $wR2 = [\sum[w(F_o^2 - F_c^2)^2]/\sum[w(F_o^2)^2]]^{1/2}$; and $w = 1/[\sigma^2F_o^2 + (AP)^2 + BP]$, $P = (F_o^2 + 2F_c^2)/3$; *A* and *B* = weight coefficients (see Supporting Information).

diffraction data.[18] Due to the limited instrument resolution, the low crystallographic symmetry, and the fairly large unit cell parameters (Table 1), the recorded powder patterns were very complex and had many overlapping peaks. This rendered the analyses of the phase purity unreliable. To circumvent this problem, a high-resolution powder diffraction pattern was taken using synchrotron radiation ($\lambda = 0.69982$ Å); for this experiment, several milligrams of β-$Ca_{21}Mn_4Sb_{18}$ crystallites carefully selected under a microscope were ground and sealed in a 0.2 mm glass capillary. Although the resolution and the intensity statistics are excellent (see Supporting Information), the unambiguous indexing of the diffraction pattern and refinement of the data are not possible. This clearly suggests the presence of impurity phase(s), most likely $Ca_{14}MnSb_{11}$[15] and MnSb.[19]

Single-Crystal X-ray Diffraction. Single crystals of the title compounds were selected in a glove box and cut in Paratone N oil to a suitable size for data collection, dimensions: 0.11 × 0.09 × 0.08 mm^3 for $Ca_{21}Mn_4Bi_{18}$ and 0.10 × 0.06 × 0.06 mm^3 for β-$Ca_{21}Mn_4Sb_{18}$. They were then mounted on glass fibers and quickly placed under the cold nitrogen stream (ca. −153 °C) of the goniometer of a Bruker SMART CCD-based diffractometer. Intensity data covering the full sphere of the reciprocal space were collected in four batch runs at different ω and ϕ angles. The frame width was 0.4° in ω and θ, and the acquisition rate was 15 s/frame ($T_{min}/T_{max} = 0.654$ and $R_{int} = 0.0511$ for $Ca_{21}Mn_4Bi_{18}$; $T_{min}/T_{max} = 0.702$ and $R_{int} = 0.0591$ for β-$Ca_{21}Mn_4Sb_{18}$). The data collection, data integration, and cell refinement were done using SMART and SAINT programs,[20] respectively. SADABS was used for semiempirical absorption correction based on equivalents.[21] The structures were subsequently solved by direct methods and refined by full matrix least-squares on F^2 using SHELXL.[22] Site occupations were checked for deviations from unity by freeing the site occupancy factor (SOF) of an individual atom while the remaining SOFs were kept fixed, which proved all sites are fully occupied. In the last refinement cycles, all atoms were refined with anisotropic displacement parameters. For the sake of uniformity with the already published structures of α-$Ca_{21}Mn_4Sb_{18}$ and $Sr_{21}Mn_4Sb_{18}$, the coordinates and the labels of the atomic positions were assigned accordingly. The refinements confirmed ordered structures with very reasonable anisotropic displacement parameters and interatomic distances. Further details of the data collection and structure refinement parameters are given in Table 1. Selected bond distances and angles for $Ca_{21}Mn_4Bi_{18}$ and for β-$Ca_{21}Mn_4Sb_{18}$ are listed in Tables 2 and 3, respectively. Final positional and equivalent isotropic displacement parameters and graphical representations of the structures with anisotropic displacement parameters are provided as Supporting Information, Tables S1 and S2, and Figures S2 and S3, respectively. Additional information in the form of CIF has also been supplied as Supporting Information, and the CIFs have been deposited with Fachinformationszentrum Karlsruhe, 76344 Eggenstein-Leopoldshafen, Germany, (fax: (49) 7247-808-666; e-mail: crysdata@fiz.karlsruhe.de)—depository number CSD 416520 ($Ca_{21}Mn_4Bi_{18}$) and CSD 416972 (β-$Ca_{21}Mn_4Sb_{18}$).

Magnetic Susceptibility Measurements. Magnetization field and zero-field cooling measurements were performed in a Quantum Design MPMS SQUID magnetometer. The samples were prepared in the glove box by carefully selecting crystals under a microscope. Because of the samples' sensitivity to air and moisture, the crystals were contained in a specially designed holder. It is made of 150−160 mm long fused silica tubing (3 mm i.d. × 4 mm o.d.) and two half-length pieces of 3 mm fused silica rods. One of the rods is inserted all the way into the tubing, and the ends of tubing and rod are flame-sealed together. The holder is then brought inside the glove box where the sample is weighed and loaded from the open end. To hold the material in place and to close the tube, the other piece of tightly fitting rod is then inserted. Subsequently, the second end is flame-sealed as well. The holder's diamagnetic contribution to the magnetization was taken into account when raw data were converted to molar susceptibility.

Electronic Structure Calculations. Electronic structure calculations for $Ca_{21}Mn_4Bi_{18}$ were performed using the linear muffin-tin orbital (LMTO) method[23] with the aid of the TB-LMTO program.[24] The basis set included the 4s, 4p, and 3d orbitals for Ca and Mn and 6s, 6p, 6d, and 4f orbitals for Bi. Exchange and correlation were treated in a local density approximation (LDA).[25] All relativistic effects except for spin−orbit coupling were taken into account by a scalar relativistic approximation.[26] All spin-polarized calculations were checked for convergence of energies, integrated COHP values, and magnetic moments. Atomic sphere radii used in the TB-LMTO-ASA calculations were chosen using an automated procedure, and interstitial spheres had been inserted to achieve the space filling automatically.[27] The *k*-space integrations were performed by the tetrahedron method[28] and a total of eight irreducible *k*-points in the Brillouin zone were used. The Fermi level was selected as the energy reference ($\epsilon_F = 0$ eV).

(18) (a) *JADE Version 6.5*; Materials Data, Inc.: Livermore, CA, 2003. (b) Larson, A. C.; von Dreele, R. B. *GSAS-General Structure Analysis System*; LAUR 86-748., Los Alamos National Laboratory: Los Alamos, NM, 1986.
(19) Villars, P.; Calvert, L. D. *Pearson's Handbook of Crystallographic Data for Intermetallic Phases*, 2nd ed.; American Society for Metals: Materials Park, OH, 1991.
(20) *Bruker SMART and SAINT*; Bruker AXS, Inc.: Madison, WI, 2002.
(21) Sheldrick, G. M. *SADABS*; University of Göttingen: Göttingen, Germany, 2003.
(22) Sheldrick, G. M. *SHELXTL*; University of Göttingen: Göttingen, Germany, 2001.
(23) (a) Andersen, O. K. *Phys. Rev. B* **1975**, *12*, 3060−3083. (b) Andersen, O. K.; Jepsen, O. *Phys. Rev. Lett.* **1984**, *53*, 2571−2574. (c) Andersen, O. K. *Phys. Rev. B* **1986**, *34*, 2439−2449. (d) Skriver, H. L. *The LMTO Method*; Springer, Berlin, 1984.
(24) Jepsen, O.; Andersen, O. K. *The Stuttgart TB-LMTO Program, Version 4.7*.
(25) von Barth, U.; Hedin, L. *J. Phys. C* **1972**, *5*, 1629−1642.
(26) Koelling, D. D.; Harmon, B. N. *J. Phys. C* **1977**, *10*, 3107−3114.
(27) Jepsen, O.; Andersen, O. K. Z. *Phys. B* **1995**, *97*, 35−47.
(28) Blöchl, P. E.; Jepsen, O.; Andersen, O. K. *Phys. Rev. B* **1994**, *49*, 16223−16233.

Table 2. Important Bond Distances (Å) and Angles (deg) within the Polyanionic Subnetwork of $Ca_{21}Mn_4Bi_{18}$

Bi1−	Mn1	2.876(2)	Mn1−	Bi1 × 2	2.876(2)
Bi2−	Mn2	2.797(2)		Bi2 × 2	2.878(2)
	Mn1	2.878(2)	Mn2−	Bi2 × 2	2.797(2)
Bi3−	Mn3	2.882(2)		Bi3 × 2	2.981(2)
	Mn2	2.981(2)		Mn3	2.797(6)
Bi4−	Mn3	2.848(2)	Mn3−	Bi4 × 2	2.848(2)
	Mn4	2.942(2)		Bi3 × 2	2.882(2)
Bi5−	Mn4	2.812(2)		Mn2	2.797(6)
Bi6−	Bi6	3.057(1)		Mn4	2.823(6)
Bi7−	Bi7	3.073(1)	Mn4−	Bi5 × 2	2.812(2)
Bi8−				Bi4 × 2	2.942(2)
Bi9−				Mn3	2.823(6)

Bi1−Mn1−Bi2	110.67(2)	Bi4−Mn4−Bi4	118.29(12)
Bi2−Mn1−Bi2	102.27(12)	Bi4−Mn4−Bi5	106.76(2)
Bi2−Mn2−Bi2	106.48(13)	Bi4−Mn4−Bi5	110.69(2)
Bi2−Mn2−Bi3	110.12(2)	Bi5−Mn4−Bi5	102.54(11)
Bi2−Mn2−Bi3	105.01(2)		
Bi3−Mn2−Bi3	119.49(13)	Mn1−Bi2−Mn2	75.62(9)
Bi3−Mn3−Bi3	126.58(14)	Mn2−Bi3−Mn3	56.96(9)
Bi3−Mn3−Bi4	102.08(2)	Mn3−Bi4−Mn4	58.37(9)
Bi3−Mn3−Bi4	101.89(2)		

Table 3. Important Bond Distances (Å) and Angles (deg) within the Polyanionic Subnetwork of β-$Ca_{21}Mn_4Sb_{18}$

Sb1−	Mn3	2.780(3)	Mn1−	Sb4	2.734(2)
Sb2−	Sb2	2.875(2)		Sb5	2.763(2)
Sb3−	Mn2	2.729(2)		Sb7	2.765(2)
	Mn3	2.783(2)		Sb11	2.902(2)
Sb4−	Mn2	2.723(3)	Mn2−	Sb4	2.723(3)
	Mn1 × 2	2.734(2)		Sb3 × 2	2.729(2)
Sb5−	Mn1 × 2	2.763(2)		Sb8	2.800(3)
Sb6−	Sb6	2.902(2)		Mn3	2.823(3)
Sb7−	Mn1	2.765(2)	Mn3−	Sb1	2.780(3)
Sb8−	Mn2	2.800(3)		Sb3 × 2	2.783(2)
	Sb8	2.837(2)		Sb10	2.781(3)
Sb9−				Mn2	2.823(3)
Sb10−	Mn3	2.781(3)			
Sb11−	Mn1	2.902(2)			
Sb12−	Sb12	2.844(2)			
Sb13−					
Sb14−					

Sb4−Mn1−Sb5	95.95(7)	Sb1−Mn3−Sb3	108.38(6)
Sb4−Mn1−Sb7	108.09(6)	Sb3−Mn3−Sb3	115.25(9)
Sb5−Mn1−Sb7	107.40(6)	Sb1−Mn3−Sb10	105.90(9)
Sb7−Mn1−Sb11	121.75(8)	Sb3−Mn3−Sb10	109.26(6)
Sb11−Mn1−Sb5	111.87(6)		
Sb4−Mn2−Sb3	112.22(6)	Mn1−Sb4−Mn1	84.46(9)
Sb3−Mn2−Sb3	118.96(9)	Mn1−Sb5−Mn1	83.39(9)
Sb4−Mn2−Sb8	82.01(7)	Mn2−Sb3−Mn3	61.60(7)
Sb3−Mn2−Sb8	112.84(6)	Mn2−Sb8−Sb8	107.44(8)

Results and Discussion

Structure and Bonding of $Ca_{21}Mn_4Bi_{18}$. $Ca_{21}Mn_4Bi_{18}$ is a new ternary compound in the Ca−Mn−Bi system, and it crystallizes with the recently reported α-$Ca_{21}Mn_4Sb_{18}$ type.[10] Since the important features of this structure type have already been discussed, the structure description provided herein will focus on a few specific details only and on the apparent structural relationship between $Ca_{21}Mn_4Bi_{18}$ and the hypothetical $Ca_{22}Mn_2Bi_{18}$ (i.e., $Ca_{11}MnBi_9$ with the $Ca_{11}InSb_9$ type[19]).

$Ca_{21}Mn_4Bi_{18}$ crystallizes in the monoclinic space group *C*2/*c* (Table 1), and its structure contains 9 bismuth, 4 manganese and 11 calcium atoms in the asymmetric unit (Supporting Information, Table S1). The implication of that is clearly visible from Figure 1—the structure seems fairly complicated, especially at a first sight. The most remarkable feature of the structure is the large $[Mn_4Bi_{10}]$ cluster anion, made up of four Mn-centered tetrahedra of Bi atoms, which are joined together along the *b* axis through sharing opposing edges, as shown in Figure 2. The Bi−Mn bond distances range from 2.812(2) to 2.981(2) Å and compare well with those reported for other ternary manganese-bismuth phases; for example, the Bi−Mn contacts in the isolated $[MnBi_4]$ tetrahedra in $A_{14}MnBi_{11}$ (A = Ca, Sr, Ba, Yb) vary from 2.814(1) to 2.935(1) Å;[15] the Bi−Mn distances in $Ca_9Mn_4Bi_9$ with $[Mn_4Bi_9]$ ribbons range from 2.827(5) to 2.974(11) Å.[8] There are also isolated Bi anions and dumbbell-shaped $[Bi_2]$ units, which are common motifs in the crystal chemistry of many pnicogen-based phases.[9,10,15] The structure also contains Ca^{2+} cations, which fill the space between the anionic species and counterbalance the charges. Hence, following the Zintl reasoning[14] and assuming a d^5 state for the manganese atoms (i.e., Mn^{2+}, confirmed by the LMTO calculations), the electron count can be rationalized as 21 Ca^{2+} cations, 4 Bi^{3-} anions, 2

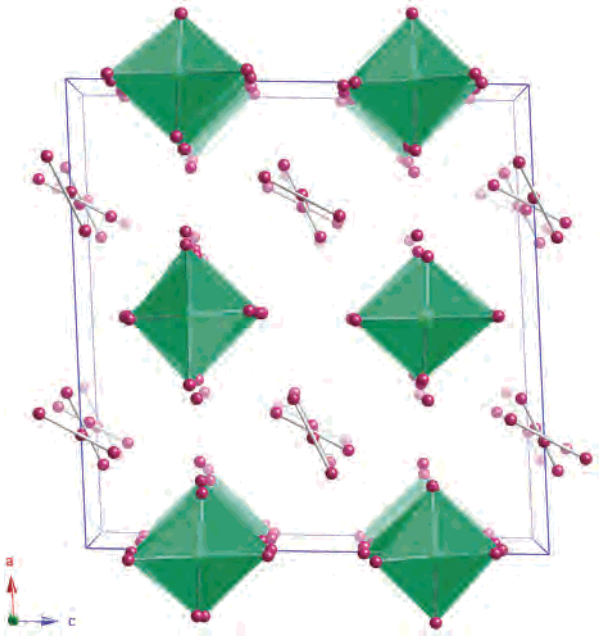

Figure 1. Polyhedral view of the structure of $Ca_{21}Mn_4Bi_{18}$, viewed down the *b* axis. The Bi atoms are drawn as red spheres, and the Mn atoms are shown with small light-green spheres inside the translucent Mn-centered tetrahedra, respectively. Ca atoms are omitted for clarity, and the unit cell is outlined.

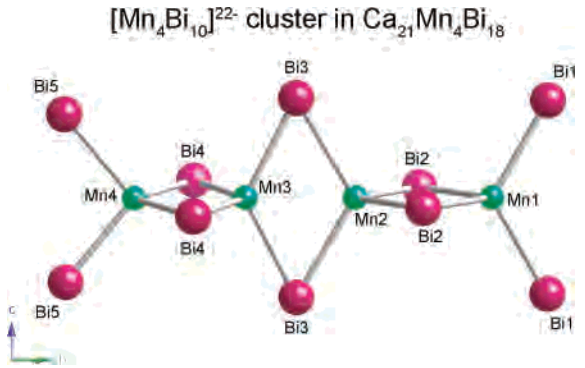

Figure 2. Detailed drawing of the $[Mn_4Bi_{10}]^{22-}$ heteronuclear cluster in $Ca_{21}Mn_4Bi_{18}$, viewed in projection nearly perpendicular to the *b* axis. Relevant bond distances and angles are listed in Table 2.

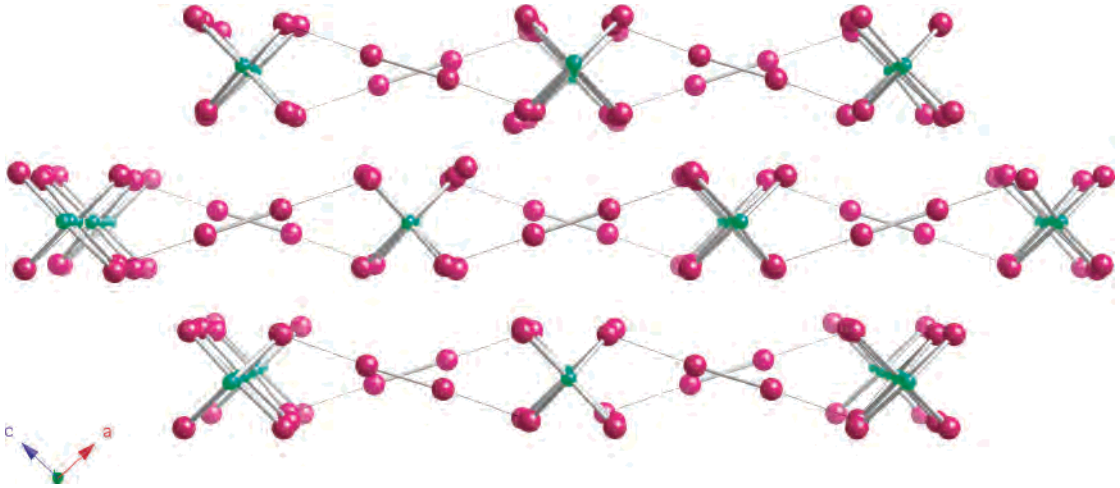

Figure 3. Structure of $Ca_{21}Mn_4Bi_{18}$ in a different representation—the $[Bi_2]^{4-}$ dimers interconnect the $[Mn_4Bi_{10}]^{22-}$ tetramers to form layers, propagating approximately parallel to the direction of the [101] planes and stacked in a "ABAB"-type fashion. Color code as in Figure 1.

$[Bi_2]^{4-}$ dimers, and 1 $[Mn_4Bi_{10}]^{22-}$ cluster anion per formula, i.e., a typical Zintl phase.

The $[Mn_4Bi_{10}]^{22-}$ linear tetramers are well separated from one another (distances between the closest Mn atoms from adjacent clusters are greater than 8 Å); however, there are some Bi−Bi contacts between them and $[Bi_2]^{4-}$ dimers, which provide for another way to visualize the structure (Figure 3). These occur between the Bi6 and Bi7 atoms from the dimers and Bi2 and Bi5 atoms of the $[Mn_4Bi_{10}]^{22-}$ anions, 3.5405(9) Å for Bi2−Bi7 and 3.6037(9) Å for Bi5−Bi6. Such contacts are arguably too long to represent significant bonding but are only slightly longer than the Bi−Bi distances (from 3.335 to 3.498 Å) in the related $A_{14}MnBi_{11}$ compounds (A = Ca, Sr, Ba)[15] or than the interlayer distances in elemental Bi (d = 3.517 Å).[29] From that perspective, if these interactions are considered as weakly bonding, the anionic part of the structure can alternatively be viewed as a 2D network depicted in Figure 3—the $[Bi_2]^{4-}$ dimers interconnect the $[Mn_4Bi_{10}]^{22-}$ tetramers to form layers, propagating approximately parallel to the direction of the [101] planes and stacked in a "ABAB"-type fashion. The Bi−Bi distances within the dimers (d = 3.057(1) Å for Bi6−Bi6, and d = 3.073(1) Å for Bi7−Bi7), in turn, compare very well with the intralayer distances in rhombohedral Bi (d = 3.064 Å),[29] and with the Bi−Bi distances within the zigzag chains of the recently reported Zintl phase $Ba_{11}Cd_8Bi_{14}$ (d = 3.055(2) Å).[30]

Another remarkable characteristic of the $[Mn_4Bi_{10}]^{22-}$ tetramer is that the four Mn centers are not equally spaced. As shown in Figure 2, the distances are: 3.480(5) Å for Mn1···Mn2, 2.797(5) Å for Mn2···Mn3, and 2.825(5) Å for Mn3···Mn4, all of which are a bit longer compared to the corresponding pairs in α-$Ca_{21}Mn_4Sb_{18}$ (due to the larger atomic size of Bi compared to Sb of course). In α-$Ca_{21}Mn_4Sb_{18}$, the shortest Mn···Mn contact is between Mn3 and Mn4,[10] whereas in $Ca_{21}Mn_4Bi_{18}$, it is Mn2···Mn3 (the adopted nomenclature for the labels is the same in both cases). This is most certainly due to distortions of the larger $MnBi_4$ tetrahedra (compared to $MnSb_4$), particularly around the Ca atom (Ca11 in the atomic list), lying in the same *ab* and *bc* planes as the four manganese atoms. The peculiarities with respect to the "bridging" Ca atom have already been noted on the example of α-$Ca_{21}Mn_4Sb_{18}$; below we point out another important structural relationship associated with this site.

Perhaps the most out of the ordinary feature of the $Ca_{21}Mn_4Bi_{18}$ structure is in the way it is related to the structure of the hypothetical compound $Ca_{11}MnBi_9$ ($Ca_{11}InSb_9$ type,[19] Pearson's symbol o*I*84, space group *Iba*2). Since many "11-1-9" phases are known already and since structure description has been given in several earlier publications,[31] further specifics of the $A_{11}TrPn_9$ compounds (Tr = triel, group 13 element; Pn = pnicogen) will not be considered herein. For the sake of clarity only, we point out the conventional way of describing their structures, namely, as built of discrete Tr-centered tetrahedra of Pn ($[TrPn_4]^{9-}$), isolated Pn dimers ($[Pn_2]^{4-}$), and isolated Pn^{3-} anions. The divalent cations, which occupy the empty space between them, counterbalance the charges, just like in the structure of $Ca_{21}Mn_4Bi_{18}$, i.e., they are all salt-like Zintl phases.

Upon careful examination, a striking similarity between the $Ca_{21}Mn_4Bi_{18}$ and $Ca_{11}MnBi_9$ structures become apparent. This is interesting because the space groups in which $Ca_{11}MnBi_9$ and $Ca_{21}Mn_4Bi_{18}$ crystallize are not related by the crystallographic group−subgroup relations—as shown in Figure 4, the isolated $[MnBi_4]^{10-}$ tetrahedra in $Ca_{11}MnBi_9$ (reformulated as $Ca_{22}Mn_2Bi_{18}$ for convenience) are bridged by specially positioned Ca cations along the direction of the *c* axis (Wyckoff site 4*a* in *Iba*2). They are at the center of distorted octahedra of Bi atoms, four of which are the vertices of neighboring $[MnBi_4]^{10-}$ tetrahedra and two are isolated Bi^{3-} anions. Very similar is the coordination of Ca11

(29) Cucka, P.; Barrett, C. S. *Acta Crystallogr.* **1962**, *15*, 865−872.
(30) Xia, S.-Q.; Bobev, S. *Inorg. Chem.* **2006**, *45*, 7126−7132.
(31) (a) Cordier, G.; Schäfer, H.; Stelter, M. Z. *Naturforsch. B: Chem. Sci.* **1985**, *40*, 868−871. (b) Cordier, G.; Schäfer, H.; Stelter, M. Z. *Anorg. Allg. Chem.* **1984**, *519*, 183−188. (c) Young, D. M.; Kauzlarich, S. M. *Chem. Mater.* **1995**, *7*, 206−209. (d) Bobev, S.; Fritsch, V.; Thompson, J. D.; Sarrao, J. L.; Eck, B.; Dronskowski, R.; Kauzlarich, S. M. *J. Solid-State Chem.* **2005**, *178*, 1071−1079.

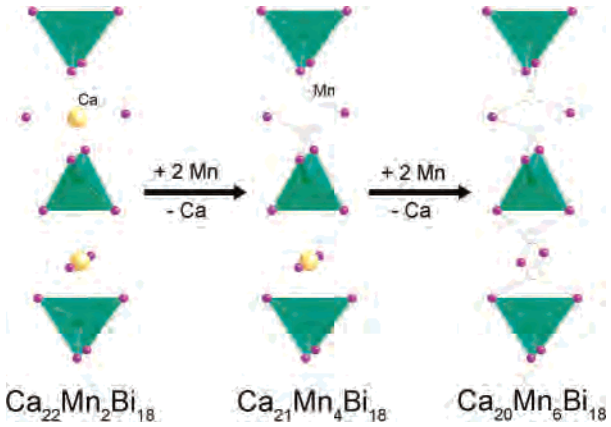

Figure 4. Schematic representation of how the structure of $Ca_{21}Mn_4Bi_{18}$ can be related to the hypothetical structures of $Ca_{22}Mn_2Bi_{18}$ and $Ca_{20}Mn_6Bi_{18}$. The formal derivation of the $[Mn_4Bi_{10}]^{22-}$ and the $[Mn_6Bi_{12}]^{24-}$ anions through removal of bridging Ca and addition of extra Mn is emphasized (see text for details).

(Wyckoff site 4*e* in *C*2/*c*) in the structure of $Ca_{21}Mn_4Bi_{18}$, as described above. In the latter situation, the linear $[Mn_4Bi_{10}]^{22-}$ anions are bridged by Ca cations along the direction of the *b* axis (Figure 1). More interestingly, from the side-by-side comparison of the two (Figure 4), it is clear that the formal removal of every second bridging Ca in the structure of the hypothetical compound $Ca_{22}Mn_2Bi_{18}$ and the addition of two Mn atoms around the vacant spot, will yield a new structure that will have the very same $[Mn_4Bi_{10}]^{22-}$ tetramers, coordinated by Ca in the very same fashion as in $Ca_{21}Mn_4Bi_{18}$. Following that scheme, it is conceivable that a subsequent removal of the bridging Ca in $Ca_{21}Mn_4Bi_{18}$ and the addition of two more Mn atoms, if possible, will result in the formation of infinite chains of edge-shared $[MnBi_4]^{10-}$ tetrahedra (Figure 4). The formula of such hypothetical compound will be $Ca_{20}Mn_6Bi_{18}$ (including the $[Bi_2]^{4-}$ dimers and the isolated Bi^{3-}). Although no such compound is known so far, there are other Zintl compounds, whose structures feature such one-dimensional chains of edge-shared tetrahedra, such as $[AlAs_2]$ in Na_3AlAs_2 for example.[32]

These considerations prompt the attention to another interesting observation regarding the formal electron count in the series of compounds discussed above. For that matter, following the Zintl rules for electron counting,[14] the formula unit of $Ca_{22}Mn_2Bi_{18}$ can be broken down to 22 Ca^{2+} cations, 2 $[MnBi_4]^{10-}$ tetrahedra, 2 $[Bi_2]^{4-}$ dimers, and 6 isolated Bi^{3-} anions. The structure of $Ca_{21}Mn_4Bi_{18}$ can be rationalized similarly as 21 Ca^{2+} cations, 1 $[Mn_4Bi_{10}]^{22-}$ linear tetramer, 2 $[Bi_2]^{4-}$ dimers, and 4 isolated Bi^{3-} anions, whereas the structure of $Ca_{20}Mn_6Bi_{18}$ has to be regarded as 20 Ca^{2+} cations, 6 $[MnBi_2]^{4-}$ linear chains, 2 $[Bi_2]^{4-}$ dimers, and 2 isolated Bi^{3-} anions.

From above, it is evident that charge neutrality can be achieved only for $Ca_{21}Mn_4Bi_{18}$. Such conclusion, although based on the overly simplistic Zintl concept is nicely supported by the band structure calculations, which show a narrow gap at the Fermi level (below). In contrast, $Ca_{22}Mn_2Bi_{18}$ and $Ca_{20}Mn_6Bi_{18}$ are 2-electron deficient and 2-electron rich, respectively. This could explain the inability to synthesize transition metal analogs of the $A_{11}TrPn_9$ compounds in which the tetrahedrally coordinated Tr^{3+} atoms are to be substituted by transition metals with half-filled (Mn^{2+}) or completely filled (Zn^{2+} or Cd^{2+}) d shells.

(32) Cordier, G.; Ochmann, H. Z. *Naturforsch. B: Chem. Sci.* **1988**, *43*, 1538−1540.

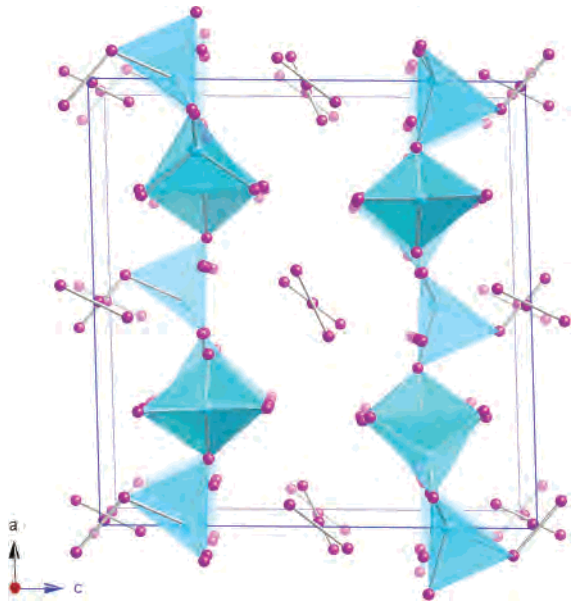

Figure 5. Polyhedral view of the structure of β-$Ca_{21}Mn_4Sb_{18}$, viewed down the *b* axis. The Sb atoms are drawn as purple spheres, and the Mn atoms are shown with small light-blue spheres inside the translucent Mn-centered tetrahedra, respectively. Ca atoms are omitted for clarity and the unit cell is outlined.

Structure and Bonding of β-$Ca_{21}Mn_4Sb_{18}$. $Ca_{21}Mn_4Sb_{18}$ reported herein is a different form of the already known $Ca_{21}Mn_4Sb_{18}$ (i.e., α-$Ca_{21}Mn_4Sb_{18}$).[10] The new β-$Ca_{21}Mn_4Sb_{18}$ polymorph crystallizes in the monoclinic space group *C*2/*m* (Table 1), and it is isostructural with another related compound, $Sr_{21}Mn_4Sb_{18}$.[9] The structure contains 14 antimony, 3 manganese, and 11 calcium atoms in the asymmetric unit, and a perspective view of this complicated structure is shown in Figure 5. Its most unique aspect is the large heteronuclear $[Mn_8Sb_{22}]^{48-}$ anion (Figure 6). It is made of three crystallographically unique $[MnSb_4]^{10-}$ tetrahedra, which share both an edge and a corner. A fourth tetrahedron generated via mirror symmetry accounts for a half of the cluster, i.e., $[Mn_4Sb_{11}]^{25-}$. Note that this unit is not linear as in the structure of the α-$Ca_{21}Mn_4Sb_{18}$ polymorph (*C*2/*c*) and can be considered as two edge-shared $[Mn_2Sb_6]$ subunits that are joined together through a common vertex, Sb4 in the current notation (Figure 6). This results in an unusual "three-coordinated" Sb atom, lying almost in the plane formed by the three next nearest Mn atoms. Because of this "strain", the shortest Mn−Sb distances and the greatest distortions from the ideal tetrahedral geometry (Table 3) are found around this Sb position and the adjacent Mn2.

Another difference between the two polymorphs is that here the $[Mn_4Sb_{11}]^{25-}$ tetramers are not isolated but rather linked to each other through external Sb−Sb bonds (2.837(2)Å) to form very large $[Mn_8Sb_{22}]^{48-}$ cluster anions. They are again well separated from each other, but the closest Mn

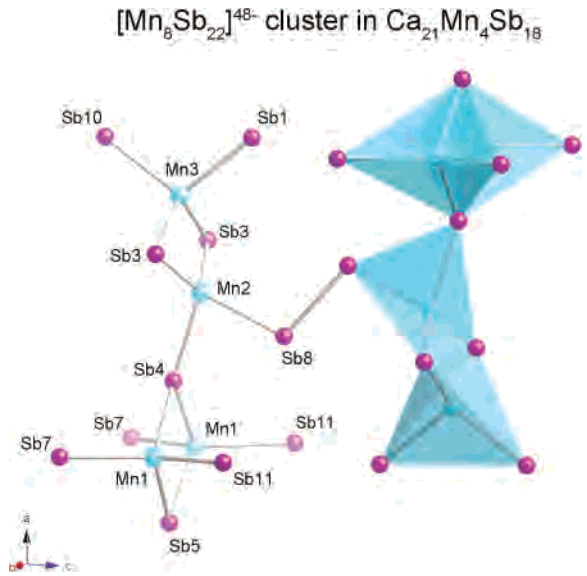

Figure 6. Detailed drawing of the $[Mn_8Sb_{22}]^{48-}$ cluster anion in β-$Ca_{21}Mn_4Sb_{18}$, viewed in projection approximately along the *b* axis. Relevant bond distances and angles are listed in Table 3.

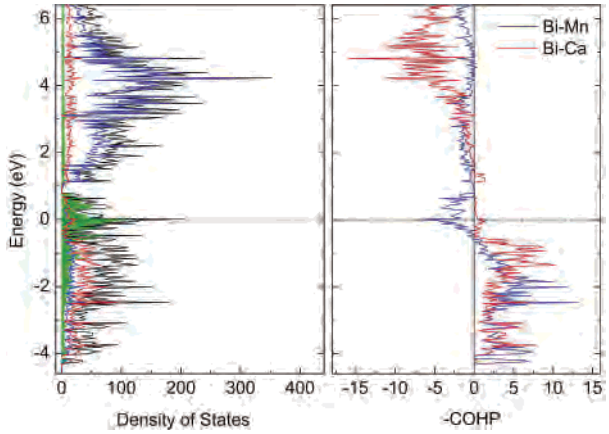

Figure 7. DOS (left) and COHP (right) diagram from nonmagnetic calculations on $Ca_{21}Mn_4Bi_{18}$. The TDOS is shown as solid black line, the PDOS for Ca and Bi are drawn with blue and red solid lines, respectively. For better contrast, the PDOS for Mn is represented with a green shaded area.

contacts between neighboring clusters are a little over 6.5 Å—much shorter compared to the α-polymorph with the linear tetramers.[10] Within the $[Mn_8Sb_{22}]^{48-}$ cluster itself, the Mn atoms are not equally spaced, just like in the $[Mn_4Sb_{10}]^{22-}$ unit in α-$Ca_{21}Mn_4Sb_{18}$. The shortest Mn···Mn distance occurs between Mn2 and Mn3, 2.823(6) Å (Table 3), whereas the second shortest distance between Mn1 and its mirror image is greater than 3.6 Å. Mn1···Mn2 separation is greater than 5 Å (Figure 6).

The Mn−Sb distances in β-$Ca_{21}Mn_4Sb_{18}$ range from 2.723(3) to 2.902(2) Å (Table 3), all of which are systematically shorter than those reported in $Sr_{21}Mn_4Sb_{18}$ (2.7633(9)−3.007(1) Å).[9] Similar shortening is seen for the Mn2−Mn3 bond as well − 2.823(6) Å for β-$Ca_{21}Mn_4Sb_{18}$ vs 2.932(3) Å for $Sr_{21}Mn_4Sb_{18}$. This is an indication that the $[Mn_8Sb_{22}]^{48-}$ cluster is not very rigid and is very sensitive to the cation environment. This could be the reason why the β-$Ca_{21}Mn_4Sb_{18}$ polymorph is difficult to synthesize and why, despite all efforts, β-$Ca_{21}Mn_4Bi_{18}$ could not be prepared. Additionally, we can speculate that for both Ca−Mn−Sb and Ca−Mn−Bi systems, the β-polymorphs are relatively much less stable than the α-ones, although without more information on the corresponding phase diagrams, these considerations are not unambiguous.

The last point that deserves a special remark here is the formal electron count for β-$Ca_{21}Mn_4Sb_{18}$. Similarly to the above-mentioned $Ca_{21}Mn_4Bi_{18}$ (and the archetype α-$Ca_{21}Mn_4Sb_{18}$ of course), the Zintl concept again can be applied to rationalize the structure of β-$Ca_{21}Mn_4Sb_{18}$ assuming again a high-spin d^5 state for the manganese atoms (i.e., Mn^{2+}). According to these electron counting rules, the unit cell content (172 atoms) can be broken down to 2 $[Mn_8Sb_{22}]^{48-}$ clusters, 6 $[Sb_2]^{4-}$ dimers, and 16 Sb^{3-} anions per unit cell, which account for 168 formal negative charges. These are exactly counterbalanced by the 84 Ca^{2+} cations, which means β-$Ca_{21}Mn_4Sb_{18}$ should be a charge-balanced compound. Qualitative band-structure calculations carried out for the model compound $Ca_{21}Cd_4Sb_{18}$ (with completely filled d shell for the sake of faster computing) reveal a gap of about 0.5 eV at the Fermi level, suggesting a narrow gap semiconducting behavior. This is corroborated by the spin-polarized calculations for $Ca_{21}Mn_4Bi_{18}$ (below) and by the measured gap of 0.16 eV for α-$Ca_{21}Mn_4Sb_{18}$.[10]

In that sense, since both polymorphs are electron precise, the same formalism used earlier for deriving the α-structure from that of the hypothetical $Ca_{11}MnSb_9$ should work for β-$Ca_{21}Mn_4Sb_{18}$ as well. However, since the topology of the polyanionic network here is very different, other kinds of Ca atoms need to be removed from the parent and substituted for a pair of Mn, concomitant appropriate distortions, and this imaginary process is not easy to visualize.

Electronic Structure. The total DOS (TDOS) and different partial DOS (PDOS) based on the nonmagnetic calculation for each component are illustrated in Figure 7 (left), noting that the bands localized at very low energy are not shown in the graph for clarity. The COHP curves for Ca−Bi and Bi−Mn interactions are also shown on the same energy scales (Figure 7, right). The bands around the Fermi level are split into three groups, contributed mainly by the Bi 6p, Mn 4s, 4p, 3d, and the Ca 4s, 3d orbitals respectively. Clearly, the nonmagnetic band structure calculations show very high DOS at the Fermi level (between 120 and 200 states per eV), which also relates to the strong antibonding region coming from the Bi−Mn interactions (Figure 8, right). Recent theoretical analyses have addressed the issue of the presence of strong antibonding character at the Fermi level in nonmagnetic calculations and have suggested it to be a driving force for spin polarizations.[33] These studies pointed out the need to treat the system with spin-polarized calculations since these antibonding interactions can be relieved as a result of the exchange splitting.

Therefore, to better understand the electronic structure and the magnetic properties of $Ca_{21}Mn_4Bi_{18}$, spin-polarized

(33) (a) Landrum, G. A.; Dronskowski, R. *Angew. Chem., Int. Ed.* **2000**, *39*, 1560−1585. (b) Gourdon, O.; Bud'ko, S. L.; Williams, D.; Miller, G. J. *Inorg. Chem.* **2004**, *43*, 3210−3218. (c) Choe, W.; McWhorter, S.; Miller, G. J. Z. *Anorg. Allg. Chem.* **2002**, *628*, 1575−1580.

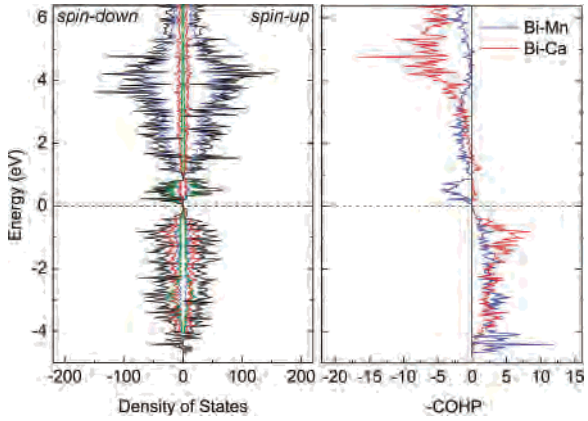

Figure 8. DOS (left) and COHP (right) diagram from antiferromagnetic calculations on $Ca_{21}Mn_4Bi_{18}$. The TDOS is shown as solid black line, the PDOS for Ca and Bi are drawn with blue and red solid lines, respectively. The PDOS for Mn is represented with a green solid line.

Table 4. Summary of Results Obtained from the Spin-Polarized Band Structure Calculations for $Ca_{21}Mn_4Bi_{18}$ Using Different Models for Magnetic Coupling (FM1 = Ferromagnetic, FM2 = Ferrimagnetic, AFM = Antiferromagnetic)

	FM1	FM2	AFM
magnetic moment on Mn1 (μ_B)	4.034	3.993	−3.899
magnetic moment on Mn2 (μ_B)	3.658	3.586	3.532
magnetic moment on Mn3 (μ_B)	3.751	−3.640	−3.645
magnetic moment on Mn4 (μ_B)	3.817	3.739	3.740
total moments ($\mu_B/Ca_{21}Mn_4Bi_{18}$)	17.630	9.136	0
ΔE_1 (eV/$Ca_{21}Mn_4Bi_{18}$)[a]	−4.324	−4.749	−5.065
ΔE_2 (eV/$Ca_{21}Mn_4Bi_{18}$)[b]	0.741	0.316	0

[a] Relative to the nonmagnetic calculation. [b] Relative to the AFM calculation.

calculations were also performed using three models for magnetic coupling within the $[Mn_4Bi_{10}]^{22-}$ linear tetramer. The calculations converged (within a 10^{-6} Ry tolerance in the total energy) to very reasonable moments on the four unique Mn atoms in the asymmetric unit, as shown in Table 4. All magnetic systems apparently have much lower total energies compared to the nonmagnetic one, which leads to a significant decrease in energy ΔE_1 (Table 4). This energy profit of at least 4 eV per formula strongly supports the arguments that the magnetic system is much more stable than the nonmagnetic one. The calculations also suggest that among the three models, the antiferromagnetic alignment of the four Mn centers is the most favorable in energy (Table 4, ΔE_2). The calculations also show considerable Mn−Mn interactions within the linear $[Mn_4Bi_{10}]^{22-}$ cluster. According to the integrated COHP values (Table S3), even the longest Mn−Mn contacts (Mn1···Mn2) represent significant bonding interactions, which are mainly originating from overlap between Mn 3d orbitals. This direct overlap between the magnetic orbitals, as evidenced from several previous theoretical studies,[34] is expected to contribute to the antiferromagnetic exchange, which is in agreement with the computational results discussed below.

The TDOS and PDOS from the spin-polarized calculations in the antiferromagnetically coupled state are presented in Figure 8. Naturally, both the DOS and the COHP differ significantly from the nonmagnetic calculations, especially near the Fermi level. The differences in the *spin-up* and *spin-down* DOS curves for either Ca or Bi are insignificant; however, the Mn 3d states are now removed from the Fermi level, and it no longer falls at a maximum of the DOS. The spin polarization also removes the Bi−Mn antibonding levels from the vicinity of the Fermi level, as clearly seen for the COHP plot (Figure 8, right). Another important difference from the nonmagnetic calculation is the narrow gap of about 0.2 eV that opens up in the DOS curve at the Fermi level. This indicates that pure $Ca_{21}Mn_4Bi_{18}$ will be a semiconductor, just like predicted following the Zintl reasoning (above). Although, because of phase purity and sensitivity to air issues we were unable to confirm this experimentally, we point out that the α-$Ca_{21}Mn_4Sb_{18}$ is a semiconductor with a band gap of 0.16 eV.[10]

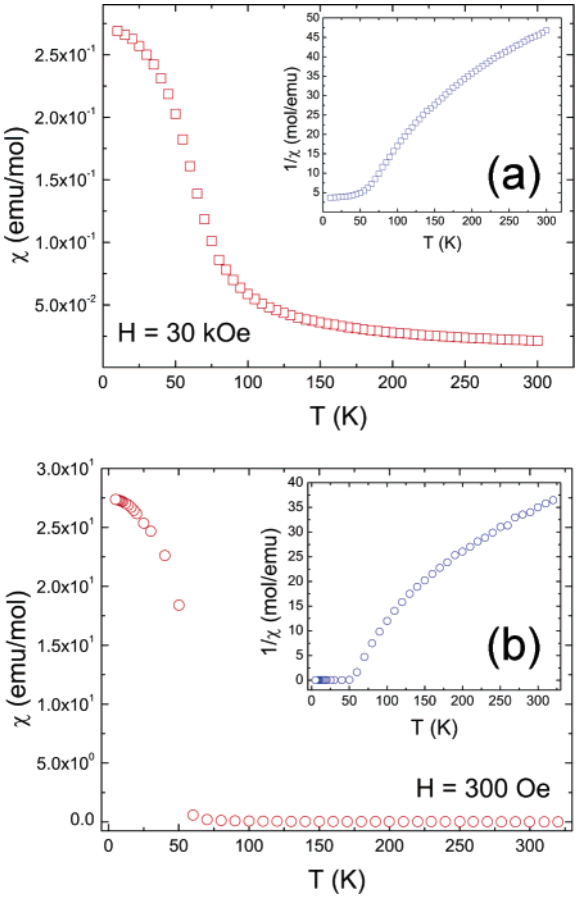

Figure 9. Temperature dependence of the dc susceptibility (χ = M/H) for polycrystalline $Ca_{21}Mn_4Bi_{18}$ measured at applied field of 30 kOe (a), and 300 Oe (b). The insets show the inverse susceptibility as a function of the temperature. A plot of the field sweep is provided as Supporting Information.

Magnetic Susceptibility. The magnetization of 12 mg of hand-selected crystallites of $Ca_{21}Mn_4Bi_{18}$ was measured in a dc mode upon cooling from room temperature down to liquid helium temperature, using an applied magnetic field of 300 Oe and 30 kOe, and the results are shown in Figure 9. Field sweeps up to 50 kOe at 5 K were carried out as well, and the corresponding plot is provided as Supporting Information (Figure S4).

(34) (a) Kahn, O. *Inorg. Chem. Acta* **1982**, *62*, 3−14. (b) Kahn, O. *Angew. Chem., Int. Ed. Engl.* **1985**, *24*, 834−850. (c) Wijngaard, J. H.; Haas, C. *Phys. Rev. B* **1992**, *45*, 5395−5405.

From the temperature dependence (Figure 9) and the field dependence of the molar magnetic susceptibility (Figure S4), it is apparent that $Ca_{21}Mn_4Bi_{18}$ orders ferromagnetically below T_c of 55 K (determined from the mid-point in the jump in $d\chi/dT$). Above T_c, and especially above ca. 150 K, the inverse susceptibility increases almost linearly with temperature, indicating that the susceptibility follows the Curie−Weiss law $\chi = C/(T - \theta_{CW})$,[35] where C is the Curie constant and θ_{CW} is the Weiss temperature. From the linear fit of the data in both plots, an effective paramagnetic moment of ca. 4 μ_B per formula unit was calculated. This value is far below what is expected for a simple spin-only system with four isolated Mn^{2+} ions in a d^5 configuration, 11.8 μ_B per formula. Moreover, the fits of the measurement at low and at high field yield largely negative values for the Weiss constants, which also significantly differ in magnitude (clearly seen from the graphs). The saturation moment of about 2 μ_B per Mn (Figure S4) is also not consistent with either antiferro- or ferromagnetic coupling. Fitting the data with the ferrimagnetic model proposed for α-$Ca_{21}Mn_4Sb_{18}$ was unsuccessful as well.[10] All of the above could indicate that the magnetic interactions in $Ca_{21}Mn_4Bi_{18}$ are very complex and that the simple spin-only models may not be accurate. In fact, the problem with the interpretation of Mn magnetism in intermetallic compounds is not new and has been a subject of a number of publications.[1−6,12,15,36] It has been shown from both theoretical and experimental point of view that even for the well-studied $A_{14}MnPn_{11}$ series, the bulk moment of about 4−5 μ_B per formula unit does not necessarily correlate with a d^4 spin state for the Mn^{3+} ion.[15] Several recent reports on compounds containing condensed $MnSb_4$ tetrahedra such as $CaMn_2Sb_2$,[12] $Sr_{21}Mn_4Sb_{18}$,[9] $Eu_{10}Mn_6Sb_{13}$,[11] or Sr_2MnSb_2[13] also suggest that many questions related to understanding the magnetism in Mn-based intermetallics are yet to be answered.

Another possible way to reconcile the magnetic susceptibility measurements with the calculation results arises if one recognizes that although the data were taken using carefully picked under the microscope crystals of $Ca_{21}Mn_4Bi_{18}$, small amounts of ferromagnetic $Ca_{14}MnBi_{11}$ impurity (always a byproduct of the reactions) could be present and could impede the measurements in a drastic way. This means that the temperature dependence of the magnetic susceptibility (Figure 9) is not that of $Ca_{21}Mn_4Bi_{18}$ but rather of the ferromagnetic $Ca_{14}MnBi_{11}$.[7] Several key arguments that support such an explanation include (1) The very strong dependence of the susceptibility with the field — the normalized molar susceptibilities (Figure 9) are different by 3 orders of magnitude, and if plotted on the same scale, the data at 30 kOe appear nearly temperature independent compared to the data taken at 300 Oe. Evidently, at 30 kOe, the ferromagnetic transition nearly "smears" out and the ferromagnetic $Ca_{14}MnBi_{11}$ phase is almost completely saturated (Figure 9a); (2) The determined critical temperature is identical to the T_c reported for $Ca_{14}MnBi_{11}$, $T_c = 55$ K;[7] (3) The effective moment is also very close to the one reported for $Ca_{14}MnBi_{11}$; (4) The strong "sample-dependence" of the measurements; and last but not least (5) The synchrotron powder diffraction data for selected crystals of β-$Ca_{21}Mn_4Sb_{18}$ (Figure S1), which prove a rather uncertain phase purity. Although circumstantial, the presented evidence has far-reaching implications since it suggests that the potential impurity phase cannot be discriminated by lower-resolution powder X-ray diffraction (most standard powder diffractometers) or detected by visual inspection of irregularly shaped "single crystals".

Hence, if an impurity-free sample of $Ca_{21}Mn_4Bi_{18}$ were to be synthesized, most likely they will exhibit weakly temperature-dependent magnetization and a low effective moment. This is in agreement with the Zintl reasoning and the electronic structure calculations, both of which predict a charge-balanced compound in which the Mn^{2+} spins are coupled antiferromagnetically with a total moment close to zero.

Conclusions

Two new ternary compounds, $Ca_{21}Mn_4Bi_{18}$ and $Ca_{21}Mn_4Sb_{18}$, have been synthesized and structurally characterized. Although the two structures are very different, both can be derived by linking $MnBi_4$ or $MnSb_4$ tetrahedra through corner- and/or edge-sharing. $Ca_{21}Mn_4Bi_{18}$ can be viewed as made up of discrete $[Mn_4Bi_{10}]^{22-}$ cluster anions, dumbbell-shaped $[Bi_2]^{4-}$ units, and isolated Bi^{3-} anions that are separated by the Ca^{2+} cations. The structure of β-$Ca_{21}Mn_4Sb_{18}$, which is the new polymorph of that compound consists of larger discrete $[Mn_8Sb_{22}]^{48-}$ anions, $[Sb_2]^{4-}$ dimers, and isolated Sb^{3-} anions, which are again separated by the Ca^{2+} cations. In $Ca_{21}Mn_4Bi_{18}$, four $MnBi_4$ tetrahedra are connected via common edges to form $[Mn_4Sb_{10}]^{22-}$ tetramers, whereas in β-$Ca_{21}Mn_4Sb_{18}$, the tetramers formed via corner- and edge-sharing are not isolated but rather linked to each other through external Sb−Sb bonds, which results in twice as large discrete $[Mn_8Sb_{22}]^{48-}$ polyanions. Electronic structure calculations show small band gaps in the DOS, which implies that $Ca_{21}Mn_4Bi_{18}$ and $Ca_{21}Mn_4Sb_{18}$ could exhibit desirable electronic and possibly thermoelectric properties. However, the lack of success in the synthesis of pure polycrystalline samples and in the growth of suitable for measurements single crystals precluded the experimental confirmation of the expected semiconducting behavior.

Acknowledgment. S.B. acknowledges financial support from the University of Delaware Research Foundation (UDRF) and from the University of Delaware through start-up grant. We also thank Prof. D. Buttrey (Department of Chemical Engineering, University of Delaware) for his assistance with the data collection at the synchrotron beam line.

(35) (a) Smart, J. S. *Effective Theories of Magnetism*; Saunders: Philadelphia, PA, 1966. (b) Kittel, C. *Introduction to Solid State Physics*, 7th Ed.; Wiley VCH: Hoboken, NJ, 1996.

(36) (a) Sánchez-Portal, D.; Martin, R. M.; Kauzlarich, S. M.; Pickett, W. E. *Phys. Rev. B* **2002**, *65*, 144414. (b) Holm, A. P.; Kauzlarich, S. M.; Morton, S. A.; Waddill, G. D.; Pickett, W. E.; Tobin, J. G. *J. Am. Chem. Soc.* **2002**, *124*, 9894−9898. (c) Wu, L.-M.; Seo, D.-K. *J. Am. Chem. Soc.* **2004**, *126*, 4398−4403. (d) Dronskowski, R. *Computational Chemistry of Solid State Materials: A Guide for Materials Scientists, Chemists, Physicists and others*; Wiley VCH: Weinheim, Germany, 2006.

Supporting Information Available: X-ray crystallographic files in CIF format (for $Ca_{21}Mn_4Bi_{18}$ and for β-$Ca_{21}Mn_4Sb_{18}$), along with detailed tables with coordinates and isotropic displacement parameters, graphical representations of the crystal structures with anisotropic displacement parameters, synchrotron powder diffraction data for β-$Ca_{21}Mn_4Sb_{18}$, plots of the field sweeps up to 50 kOe, a table with integrated COHP, and a plot of the Mn−Mn COHP. This material is available free of charge via the Internet at http://pubs.acs.org.

IC061958J